Available online at www.sciencedirect.com

SCIENCE DIRECT

Magnetic Resonance Imaging 22 (2004) 1429–1440

MAGNETIC RESONANCE IMAGING

Combination of BOLD-fMRI and VEP recordings for spin-echo MRI detection of primary magnetic effects caused by neuronal currents

Marta Bianciardi[a,b,c,d,*], Francesco Di Russo[e,f], Teresa Aprile[e,g], Bruno Maraviglia[b,c,d], Gisela E. Hagberg[a]

[a]*Laboratory of Neuroimaging, Foundation Santa Lucia I.R.C.C.S., 00179, Rome, Italy*
[b]*Department of Physics, University of Rome "La Sapienza", 00185, Rome, Italy*
[c]*National Institute for the Physics of Matter, Research Unit of Rome 1, 00185, Rome, Italy*
[d]*"Enrico Fermi" Center, 00184, Rome, Italy*
[e]*Laboratory of Neuropsychology, Foundation Santa Lucia I.R.C.C.S., 00185, Rome, Italy*
[f]*Dipartimento di Scienze della Formazione per le Attività Motorie, University of Motor Science IUSM, 00194, Rome, Italy*
[g]*Department of Psychology, University of Rome "La Sapienza", 00185, Rome, Italy*

Received 15 October 2004; accepted 15 October 2004

Abstract

In the present paper, for the first time, the feasibility to detect primary magnetic field changes caused by neuronal activity in vivo by spin-echo (SE) magnetic resonance imaging (MRI) is investigated. The detection of effects more directly linked to brain activity than secondary hemodynamic–metabolic changes would enable the study of brain function with improved specificity. However, the detection of neuronal currents by MRI is hampered by such accompanying hemodynamic changes. Therefore, SE image acquisition, rather than gradient-echo (GE) image acquisition, was preferred in the present work since the detection of primary neuronal and not blood oxygenation level-dependent (BOLD)-related effects may be facilitated by this approach. First of all, a precise spatiotemporal synchronization of image acquisition with the neuronal event had to be performed to avoid refocusing of the dephasing phenomenon during the course of the SE sequence. At this aim, we propose the combined use of visual evoked potential (VEP) recordings and BOLD-fMRI measurements prior to SE MRI scanning. Moreover, we exemplify by theory and experimentation how the control of artefactual signal changes due to BOLD and movement effects may be further improved by the experimental design. Finally, results from a pilot study using the proposed combination of VEP recordings and MRI techniques are reported, suggesting the feasibility of this method.

Keywords: Spin-echo MRI; Neuronal currents; VEP; Magnetic effects

1. Introduction

In the present paper, for the first time, the possibility to detect magnetic field effects caused by neuronal activity in vivo by spin-echo (SE) magnetic resonance imaging (MRI) is investigated. In recent MRI literature, some works explore the feasibility of detecting magnetic field changes associated with neuronal activity; these variations are more directly linked to brain functional processes than secondary hemodynamic–metabolic changes that are detectable, for instance, by blood oxygenation level-dependent (BOLD) functional MRI (fMRI). From magnetoencephalogram (MEG) studies, expected magnetic field strength variations induced locally in the presence of neuronal currents are in the order of 0.1–1 nT [1,2]. By applying currents in electric circuits positioned inside water phantoms, it has been shown that MRI has enough sensitivity to detect such small magnetic field variations (0.1–0.2 nT) along the external magnetic field, both at 3 T [2,3] and at 1.5 T [4]. Moreover, in in vitro cell cultures, magnetic field effects of spontaneous neuronal activity (at a spiking rate of about 0.15 Hz) have been detected by SE-phase MRI [5]. Despite these encouraging results, some issues such as optimization of the acquisition strategy for detection of neuronal magnetic effects and the practicability of detecting them in vivo are still of intense debate. On one hand, Konn et al. [3] have

* Corresponding author. Laboratory of Neuroimaging, Foundation Santa Lucia I.R.C.C.S., Via Ardeatina 306, 00179, Rome, Italy. Tel.: +39 06 51501547; fax: +39 06 51501213.
E-mail address: m.bianciardi@hsantalucia.it (M. Bianciardi).

0730-725X/$ – see front matter © 2004 Elsevier Inc. All rights reserved.
doi:10.1016/j.mri.2004.10.009

demonstrated in simulations of extended dipoles (spatial extent, $2\times3\times3$ mm^3) that phase images are more sensitive to weak magnetic field changes than magnitude images; besides, Bodurka and Bandettini [2] showed, for currents flowing in a circuit, that SE techniques are more suitable than gradient-echo (GE) strategies for detecting primary effects of neuronal currents, suggesting that discrimination between fast electric phenomena and other slower processes of non-neuronal origin such as movement-related artefacts and BOLD contributions to the signal may be better accomplished by SE techniques. On the other hand, the only successful pieces of experimental evidence [6,7] of a direct detection of neuronal current magnetic effects in vivo were obtained by the use of magnitude GE images.

Although knowledge of the exact geometry of the dipolar source would resolve the theoretical dichotomy related to the use of phase or magnitude images, in an experimental situation both image types are generally available and results can be compared. Dissimilarly, the choice of acquisition sequence (GE or SE) will undoubtedly impact the outcome of neuronal current MR measurements. There are several advantages associated with the SE technique. First, non-neuronal contributions to the signal that are slower than the echo time (TE), such as BOLD and some movement-related effects, are refocused and hence minimized with respect to a GE acquisition [2]. Indeed, BOLD effect sizes in SE magnitude images are lower than in GE images [8]; moreover, at high fields (>3 T), the macrovascular contribution to the signal is suppressed [8], while at low fields (1.5–3 T), intravascular dephasing effects are still the dominant contribution to the signal [9]. The SE technique as well as GE acquisitions require a careful temporal synchronization of the neuronal event with image acquisition, within a few milliseconds; in addition, in SE measurements only, symmetric time evolution of the neuronal event around the refocusing pulse must be avoided. With this aim, long echo times (TE=100–200 ms) are generally needed to accommodate the time evolution of the neuronal currents, as will be shown in the present work. Conversely, the main advantage with GE acquisitions is that there is no risk of refocusing the effect of the neuronal currents; furthermore, this technique is more suited when high scanning rates are needed [e.g., for the detection of high-frequency (>5 Hz) dipolar waves].

Generally, in vivo, discrimination between primary neuronal effects and secondary hemodynamic–metabolic changes is fundamental for a successful application of neuronal current MRI. In order to minimize any ambiguity in this respect, we preferred the use of SE acquisition for our in vivo work on a healthy subject. In order to maximize SE image contrast, methods that enable an exact temporal synchronization of the neuronal event with the MR SE acquisition had to be developed. In order to gain knowledge of the temporal dynamics of the neuronal events, electroencephalogram (EEG) recordings of visual evoked potentials (VEP) were performed for the subject under investigation—the same stimuli as for MRI were used. The SE sequence was subsequently adapted to reflect the dynamics of the dipolar sources, and information regarding the dipole geometry estimated by EEG recordings was used for positioning of the subject and for the measurement slices during the MR experiments. This approach was motivated by the fact that only magnetic field variations parallel with the external magnetic field B_0 can be detected; hence, the orientation of the dipole, in particular its orthogonality with respect to B_0, is crucial. During the course of the MR examination, besides neuronal current SE MRI, conventional BOLD GE and SE fMRI were also performed. In the present paper, we also outline some theoretical considerations regarding the experimental design used for neuronal current SE MRI and show how this can help in further optimizing the measurements. Finally, we report on a pilot study using the proposed combination of EEG and MRI techniques, assessing the possibility to control for artefactual signal changes due to BOLD and movement effects.

2. General approach

2.1. The VEP-fMRI approach for synchronizing the neuronal event with SE MR measurements

Synchronization of SE MR images with a neuronal event, which is the basis for an optimal SE MRI contrast, relies on the knowledge of specific features of the brain response (for instance, dipole time evolution and orientation) in a given subject and for a specific stimulation used in the neuronal current MRI measurement. At this aim, we introduce a method that combines information from EEG recordings of VEP and fMRI measurements that were performed separately but on the same subject and using the same stimuli. It consists of the following steps:

Prior to MRI scanning

1. *Characterization of the dipolar source*. High-resolution (64 channels) VEP recordings and estimation of the location, orientation and signal dynamics (onset, peak, duration and sign of the signal) of the dipolar sources subtending the first major VEP component (C1).

During MRI scanning

2. *Adaptation of the SE MRI sequence*. TE and stimulus timing with respect to SE MRI acquisition are adapted to reflect the dipole time evolution.
3. *Adaptation of MRI acquisition to the geometry of the dipolar source*. Optimization of patient positioning within the bore of the MR scanner in order to achieve orthogonality between dipole orientation and static magnetic field as far as possible. In this respect, specific visual stimuli known to generate dipolar sources with minor components along the static magnetic field, after subject positioning inside

the MR scanner, can be chosen. In addition, the measurement slices are oriented orthogonal to the VEP dipole and are positioned such that both VEP source and active BOLD regions are covered.

4. *Identification of activated brain regions by BOLD GE fMRI*.
5. *Synchronization of SE MR images with stimulus presentation*. During scanning, the timing of the stimuli is adapted so that the dipolar effect is not refocused during acquisition. The stimulus timing used is optimized for the detection of neuronal events rather than for hemodynamic BOLD changes in SE images (Design 1, for a theoretical background see next paragraph).
6. *Calibration of BOLD effects in neuronal current SE MRI*. Additional scans are acquired by the SE MRI technique, during presentation of stimuli with a different timing (Design 2; see next paragraph), which is suitable for the detection and hence calibration of hemodynamic BOLD changes in SE images.

The application of the described approach enables the formulation of a criteria by which assessing whether a voxel or a cluster present in a SE amplitude or phase activation map, obtained by performing Step 5, indicates the site of a neuronal event. Indeed, in case of the detection of magnetic changes induced by neuronal currents, positively or negatively activated voxels in phase images (only negative in magnitude images) should lie near a region defined as activated in the BOLD GE study (Step 4). Ideally, two such voxels—proximal to each other, one positively and another negatively correlated with the regressor describing a neuronal event—should be detected.

3. MRI detection of neuronal current effects in the presence of unwanted signal changes of non-neuronal origin

The contrast-to-noise ratio (CNR) in BOLD SE images is lower than that in GE images [8]; however, BOLD SE contributions, even if small, cannot be neglected a priori since also the neuronal response, if detectable, is expected to be weak in intensity. Therefore, at least two task-related components will contribute to the functional contrast in SE-phase and magnitude images, synchronized with the neuronal event, as described in the paragraph above, and acquired over time in a functional experiment: the BOLD hemodynamic response ($\mathbf{R}_H$) and the neuronal response ($\mathbf{R}_N$). Considering an experimental data vector $\mathbf{y}$ acquired voxel by voxel for N time points, it can be written:

$$\mathbf{y} = \mathbf{R}_H + \mathbf{R}_N + n = h\ \mathbf{M}_H + n\ \mathbf{M}_N + e \quad (1)$$

where h and n are the effect sizes of the modeled hemodynamic ($\mathbf{M}_H$) and the neuronal ($\mathbf{M}_N$) responses in the assumed linear model ($\mathbf{R}_H = h\ \mathbf{M}_H$; $\mathbf{R}_N = n\ \mathbf{M}_N$), respectively, and n and e are the actual and residual error terms, respectively.

In the context of an SE acquisition, when trying to detect neuronal effects, the only way to account for BOLD effects and hence to avoid artefacts of hemodynamic origin is given by the use of an appropriate experimental design, thus stimulus timing. Indeed, assuming that a linear model for the hemodynamic response is valid [10], $\mathbf{M}_H$ is linked directly to $\mathbf{M}_N$ by a convolution product with an assumed kernel representative of the impulsive hemodynamic response function (iHRF):

$$\mathbf{M}_H = \mathbf{M}_N \otimes \mathrm{iHRF} \quad (2)$$

so that Eq. (1) can be reformulated as follows:

$$\mathbf{y} = h\ (\mathbf{M}_N \otimes \mathrm{iHRF}) + n\ \mathbf{M}_N + e \quad (3)$$

Here we model $\mathbf{M}_N$ by a first-order Finite Impulse Response, FIR, model with a total duration of one repetition time (TR). In order to account for the BOLD effect, the stimulation timing has to be accurately designed so that the two vectors, $\mathbf{M}_N$ and $\mathbf{M}_N \otimes \mathrm{iHRF}$, become orthogonal, otherwise they will be confounded. While $\mathbf{M}_N$ is strictly linked to the stimulus timing and the FIR model, the other term ($\mathbf{M}_N \otimes \mathrm{iHRF}$) is linked to the shape of the iHRF; indeed, the impulsive hemodynamic response is a function with slow components (<0.2 Hz) accounting for the slow time-varying hemodynamic–metabolic adjustments that follow the local increase in neuronal activity. The shape of the impulsive hemodynamic response is well documented for magnitude signals acquired by GE strategies [11,12]. In magnitude SE images, it is expected to be similar to the GE, with a possible earlier onset, as recently demonstrated [13,14]; likewise, it can be shown by simulations based on a capillary vascular network [15] that the functional contrast in phase images will be similar to that in magnitude images. In the present paper, the orthogonalization of the two terms was performed in the frequency domain, hence by the use of a stimulation design (Design 1) with temporal frequency components (0.28 Hz) higher than 0.2 Hz (see Fig. 1).

In order to calibrate the intensity (statistical significance) of the hemodynamic response in Design 1, a block design, which is better suited for estimating hemodynamic responses, was used too (Design 2). Indeed, the expected effect size, h, is the same for Designs 1 and 2 (given Gaussian distributed residual errors), while an improvement of the statistical significance of the estimated effect size (in terms of its covariance) is achieved in Design 2. Expected statistical t values related to hemodynamic changes for Design 1 will be equal to the t values of Design 2 multiplied by the efficiency (E) ratio E_1/E_2 for estimating hemodynamic effects of Designs 1 and 2. Each efficiency is computed as $E = \sqrt{1/(\mathbf{X}^{+}\mathbf{X}^{+\mathrm{T}})}$, where $^{+}$ is the pseudoinverse operator and $\mathbf{X}$ is the regressor (note that t values are directly proportional to efficiency). Hence, when trying to detect neuronal effects, we also suggest to calibrate and improve the control of

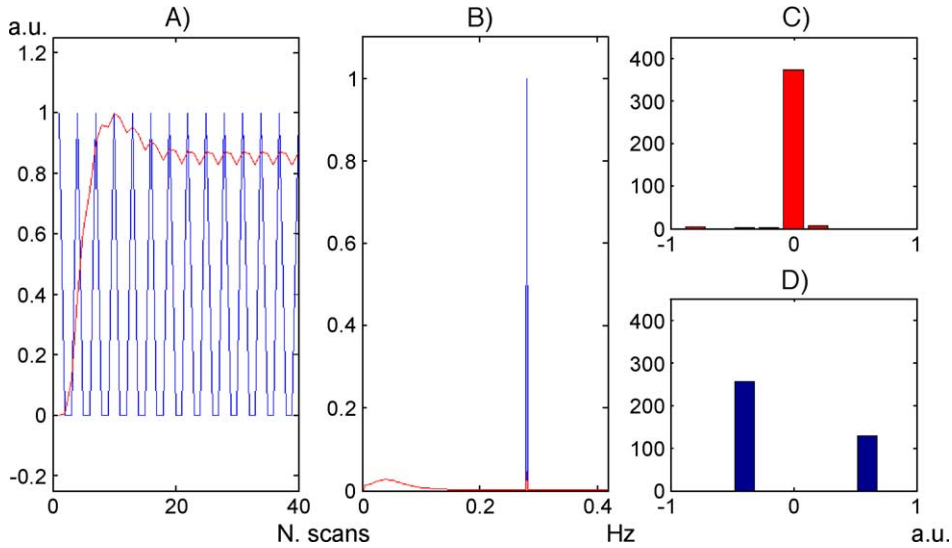

Fig. 1. Experimental design (Design 1) used for the SE MRI acquisitions and expected response time courses. Design 1 is optimized for estimation of the neuronal response and has a high stimulus frequency: 1 scan ON/2 scans OFF. In (A), details [i.e., the initial 40 scans (total equal to 384)] of the modeled neuronal ($\mathbf{M}_N$) and hemodynamic ($\mathbf{M}_H$) responses (in blue and red, respectively) are shown. In (B), the power spectral density function is shown; in (C) and (D), for $\mathbf{M}_N$ and $\mathbf{M}_H$, respectively, histograms of the temporal distribution are illustrated. Orthogonality between neuronal and hemodynamic responses is achieved for Design 1, with a correlation coefficient between the two responses equal to 0.1.

possible hemodynamic contributions in SE signals by performing additional measurements, using a design suited for estimating BOLD effects in SE images (i.e., Design 2).

Task-related unwanted contributions in the neuronal current MRI measurements other than BOLD signals may also occur due to task-related brain movement ($\mathbf{R}_M$). This issue is not dealt with in detail in this paper, except for the constriction of the $\mathbf{R}_M$ component by the use of appropriate cushioning and of a bite bar during MR acquisition.

4. Methods

4.1. Participants

One healthy subject (female, 22 years old) volunteered to participate in the study and gave her informed consent according to guidelines reviewed and approved by local ethics authorities for work involving humans.

In the VEP experiment, the subject was comfortably seated in a dimly lit sound-attenuated and electrically shielded room; in the MRI experiment, the participant had to lay supine inside the magnet bore throughout the experiment during the presentation of the visual stimuli. Positioning in the MR system was performed such that the participant's head would be approximately centered in the standing magnetic field; head movement was minimized by mild restraint and cushioning together with the use of an individually molded bite bar.

5. Apparatus

A Siemens Vision Magnetom MR system (Siemens Medical Systems, Erlangen, Germany) operating at 1.5 T and equipped for echo-planar imaging was used for acquiring MR images. A flexible surface coil (size, 37× 17 cm) was used for signal reception, while the body coil was used for radio frequency transmission.

In the MRI experiment, visual stimuli were projected via mirroring to a front projection screen using an LCD video projector (Model VPL-351QM, Sony Corp., Tokyo; refresh rate, 60 Hz) located inside the MR room; the projector was connected to a Dell Notebook CPx J750GT (600 MHz, 130.5 Mb RAM; Graphic card, ATI RAGE Mobility-M1 AGP2X, 8 Mb) located outside the MR room. Another PC (Hewlett Packard Intel Pentium, 48 Mb RAM, and software written in C^{++}, Borland version 4.52, running on MS-DOS) was used to record 5V quadratic pulses from the MR scanner; it was used also to send a counting trigger pulse to the notebook serial port for synchronization of the stimulus presentation with MRI acquisition. At specific delays after trigger delivery, the notebook started the stimulus presentation (guided by in-house software written in Cogent 2000, version 1.25). The achieved synchronization precision between MR scanning and stimulus presentation was within a few milliseconds.

MR image analyses were performed with software (see Section 10) running on LINUX (Debian 3.0) on an IBM server (xSeries 235, Intel Xeon 2.4 GHz dual processor).

In the VEP experiment, the EEG was recorded from 64 electrodes placed according to the 10–10 system montage (for details, see Ref. [16]). Visual stimuli were presented for each of the visual quadrants on a video monitor with a refresh rate of 60 Hz at a viewing distance of 57 cm; the monitor was controlled by the DOS-based STIM stimulation software (Neuroscan Inc., USA) running on a PC (Intel Pentium III, 650 MHz, 256 Mb RAM; Graphic card, ETI 6000 Direct Draw-3.50 Mb) that also tagged the EEG

acquisition. EEG recordings and VEP analysis were performed on a PC (Intel Pentium IV, 1.80 GHz, 512 Mb RAM) using the Brain Vision system (Brain Products, Germany) that includes the software Vision Recorder and Vision Analyzer.

6. Stimuli

The stimulus (Fig. 2B) consisted of a checkerboard segment (windmill) starting 3° from the fixation point and extending laterally for 14° of the visual angle (basis 9°). A central cross (0.2°) was used as fixation point. The spatial frequency was 2 cycles/degree. The background was isoluminous with the mean luminance (22 cd/m^2) of the grating pattern, which was modulated at a contrast of 32%. The center of the stimulus was displayed at polar angle of 25° above the horizontal meridian. This stimulus was binocularly presented for 50 ms in the upper left quadrant of the visual field (in the VEP experiment also in the other quadrants, for control), alternated with a stimulus with only the central fixation cross displayed.

7. VEP acquisition

Subjects were trained to maintain stable fixation on the central cross throughout stimulus presentation and reduce eye blinking as much as possible. All scalp channels were referenced to the left mastoid (M1). Horizontal eye movements were monitored with a bipolar recording from electrodes at the left and right outer canthi. Blinks and vertical eye movements were recorded with an electrode below the left eye, which was referenced to site Fp1. Each run lasted 120 s followed by a 30-s rest, with longer breaks interspersed. A total of about 18 runs was carried out in order to deliver at least 800 stimuli to each visual quadrant. The stimuli were presented at a fast rate (SOA varying between 400 and 700 ms).

The EEG was digitized from each site at 250 Hz with an amplifier bandpass filter of 0.01 to 60 Hz including a 50-Hz notch filter; impedances were kept below 5 KΩ. VEPs were stored for offline averaging epochs that began 100 ms prior to the stimulus onset and lasted for 1000 ms. Computerized artefact rejection was performed prior to signal averaging in order to discard epochs in which deviations in eye position,

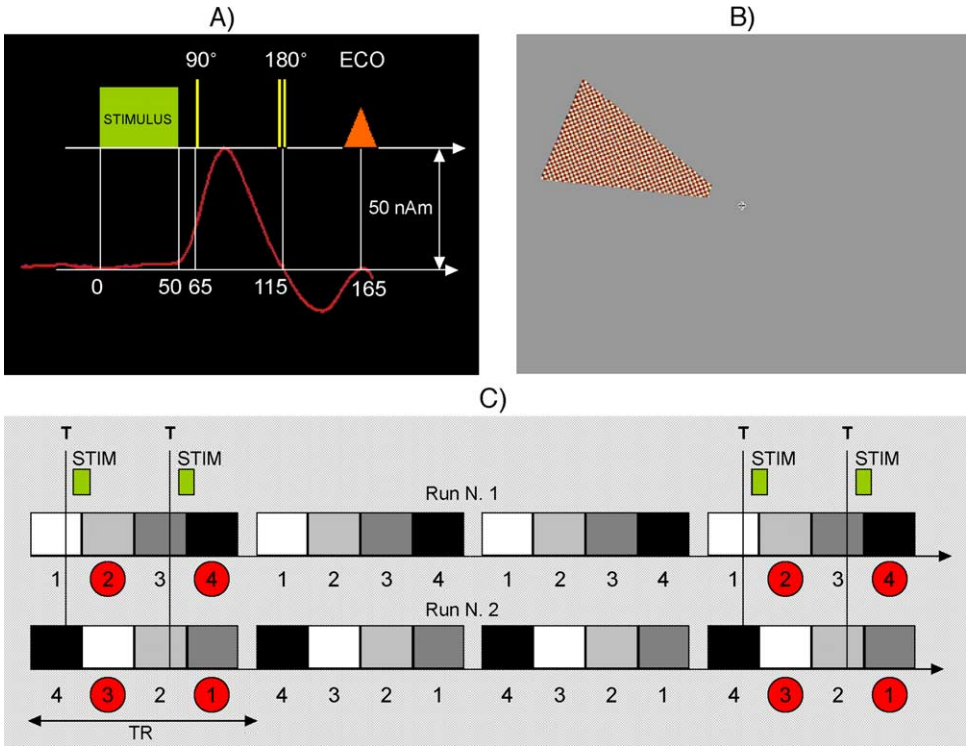

Fig. 2. Temporal synchronization of MRI acquisition and stimulus delivery. The timing of the visual stimulus was made to optimize the dipolar time evolution during MR excitation and refocusing. As shown in (A), RF pulses were temporally positioned and the TE was adapted in order to avoid refocusing of the dephasing event determined by VEP. For instance, the time evolution of the first VEP component, C1, of the subject investigated exhibits a first peak between 50 and 115 ms, while a second peak with opposite polarity and lower amplitude (between 115 and 165 ms) is also present. The TE of the MR sequence was adapted to accommodate the full-time evolution of the first VEP peak thus with an expected enhanced MRI contrast because of the positioning of the 180° RF pulse. The details of the visual stimulus are shown in (B); colored checkerboard with a central fixation cross was used for both VEP and MRI experiments. The stimulus was displayed for 50 ms and alternated by the fixation cross (shown in the center of B). As shown in (C), two different slice acquisition orders, ascending and descending, were performed in order to cover active visual areas and to improve neuronal current detection. For Design 1, the acquisition of 2 slices/scan was synchronized with stimulus (STIM) delivery; thus, during each ON period, stimulation was delivered twice, synchronized with the acquisition of a dephasing effect either in Slices 2 and 4 (ascending slice acquisition order) or in Slices 1 and 3 (descending slice acquisition order), in different runs. The MR trigger (T) was received relative to the slice preceding the slice of interest.

blinks or amplifier blocking occurred. On average, about 11% of the trials were rejected for violating these artefact criteria. To further reduce high-frequency noise, the averaged VEPs were low-pass filtered at 35 Hz.

8. fMRI acquisition

8.1. BOLD contrast in GE MRI

In order to localize activated brain regions, *GE EPI magnitude and phase images* with blipped sinusoidal read-out trains and a bandwidth per pixel of 2080 Hz were acquired with a TE of 64 ms and a TR of 3200 ms. The flip angle was set to 90°, the in-plane resolution to 3×3 mm and a total of 16 double-oblique slices (angle $\alpha_{C\rightarrow T}$, coronal to transverse, equal to −35°, −26° and $\alpha_{C\rightarrow S}$, coronal to sagittal, equal to +6° ,+6° for the first and second experimental sessions, respectively) with a thickness of 5 mm was acquired with an ascending slice order. A total of 102 EPI scans was acquired, and the first 6 of them were discarded to remove T_1 saturation effects. During image acquisition, stimuli flashing at 6.7 Hz, alternated by a stable fixation cross, were presented with a symmetric ON/OFF cycle of 20 scans' duration.

8.2. Neuronal current and BOLD contrast in SE MRI

Neuronal current and BOLD contrast SE EPI magnitude and phase images, with blipped trapezoidal read-out trains and a bandwidth per pixel of 926 Hz, were acquired in separate runs after optimization of the TE to reflect VEP dynamics. The flip angle was set to 70° and a total of 390 images with a TE of 100 ms and TR of 1.3 s was acquired. The first 6 images were discarded from further analysis to remove any possible T_1 saturation effect. The in-plane resolution and positioning of slices were the same as for the BOLD GE MRI session, but only 4 slices were acquired in a descending or ascending order. During image acquisition, the stimulus presentation was varied according to two experimental designs:

Design 1 (neuronal current detection): stimuli flashing at 1.7 Hz, alternated by a stable fixation cross, were presented with a 1 scan ON/2 scans OFF cycle. During the ON period, two stimuli were presented, each

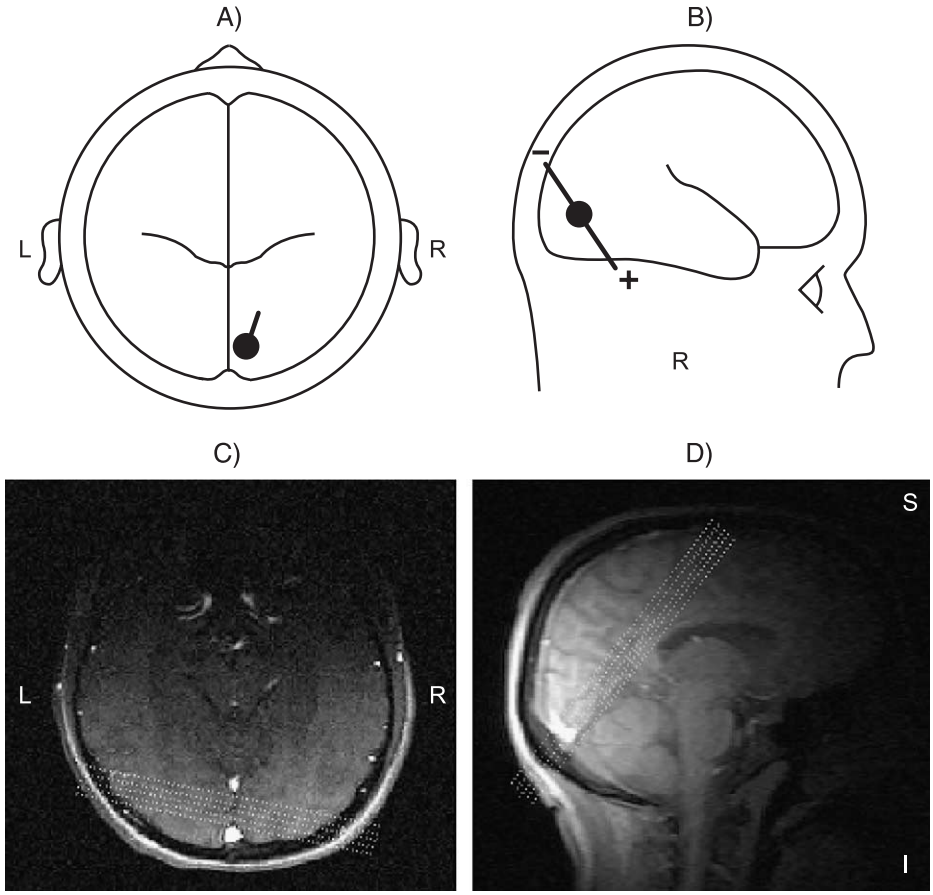

Fig. 3. Geometry of dipolar source, related to the first evoked C1 component, and optimization of positioning for MR scanning. In (A) and (B), the location and orientation of the C1 source dipole, estimated by the BESA algorithm, are superimposed on a transversal and a sagittal schematic view, respectively, of the human brain (L indicates left; R, right). In (C) and (D), experimental positioning of MR slices is shown in a transversal and a coronal view, respectively. The external static magnetic field, B_0, is oriented along the inferior–superior (I–S) direction. Perfect orthogonality between B_0 and the dipole orientation was not achieved due to physical–physiological constraints.

synchronized to two of the four slices. A total of two runs was acquired, both for ascending and descending slice orders (Fig. 2C).

Design 2 (BOLD SE MRI calibration): stimuli flashing at 1.7 Hz, alternated by a stable fixation cross, were presented with a 20 scans ON/OFF cycle. Only one run (ascending acquisition order) was performed. Since the efficiency ratio E_1/E_2 for estimating hemodynamic effects of Designs 1 and 2 is about 0.5, expected statistical t values related to hemodynamic changes for Design 1 will be half of those detected for Design 2.

The presentation of the stimuli was synchronized with MR acquisition; as outlined in Fig. 2A, appropriate delays between stimulus onset and the excitation pulse were chosen according to the dipolar source onset latency (see below) with respect to the stimulus onset. Patient positioning was performed in order to orthogonalize as far as possible the dipole orientation, estimated by the VEP recordings, to the external field B_0. Likewise, slice positioning (kept invariant during each MRI session) was performed on the basis of dipole localization (in terms of Talairach coordinates) obtained by the VEP analysis (see below) and oriented orthogonal to the dipole orientation (Fig. 3A,B), resulting in a double-oblique slice (see Fig. 3C,D).

The subject participated in two experimental MRI sessions performed on different days.

9. ERP analysis

Estimation of the dipolar sources of VEP components was carried out using Brain Electrical Source Analysis (BESA 2000 version 5.1, MEGIS Software, Germany). The BESA algorithm estimates the location and orientation of multiple equivalent dipolar sources by calculating the scalp distribution that would be obtained for a given dipole model (forward solution) and comparing it with the actual VEP distribution. Interactive changes in the location and orientation of the dipole sources lead to minimization of the residual variance between the model and the observed spatiotemporal VEP distribution (Fig. 4). This analysis used a realistic approximation of the head, with the radius equal to 90 mm. A spatial digitizer recorded the three-dimensional coordinates of each electrode and of three fiducial landmarks (the left and right preauricular points and the nasion). A computer algorithm was used to calculate the best-fit sphere that encompassed the array of electrode sites and determine their spherical coordinates. The spherical coordinates for each site were used for the topographic mapping and source localization procedures. In addition, individual spherical coordinates were related to the corresponding digitized fiducial landmarks and to landmarks identified on the standardized finite element model of BESA 2000. The first VEP component, C1, was fitted with one single dipole in the time interval from 50 to 110 ms (for more details, see Ref. [16]).

Each dipole was defined in terms of location (Talairach coordinates) and orientation (Cartesian coordinates, with the length of the vector, specified by three orientation coordinates, equal to unity) and time course (dipole moment). Onset, peak and offset latencies were then established for the component of interest, C1.

10. MRI analysis

Movement artefacts were assumed negligible since motion correction parameters did not exceed 1 mm for translations and 0.5° for rotations.

Phase image preprocessing was performed with a software developed in Matlab, version 6.0 (The MathWorks,

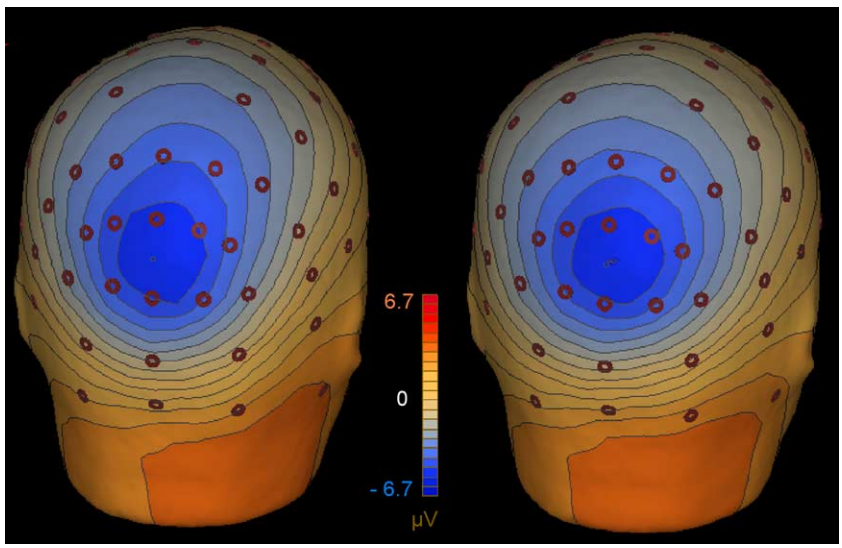

Fig. 4. Observed (left) and estimated (right) scalp VEP topography at 80 ms after stimulation onset relative to the subject investigated in the study and the first visual evoked component C1. As visible, the spatial distributions estimated by the BESA algorithm are in optimal agreement with the VEP measurements.

Inc., Natick, MA, USA); each phase time series was temporally unwrapped and then linearly detrended.

Both magnitude and phase images were then analyzed by SPM2 (Statistical Parametric Mapping, Wellcome Department of Imaging Neuroscience, London, UK, http://www.fil.ion.ucl.ac.uk/spm/spm2.html).

BOLD GE EPI magnitude images were spatially smoothed (FWHM=6 mm) and temporally regularized for colored noise; high-pass temporal filtering, with cutoff frequency v_C equal to 1/128 Hz, was applied, followed by autocorrelation estimation of the residuals, assuming a first-order autoregressive model plus white noise. Linear regression with only the modeled hemodynamic response, $\mathbf{M}_H$, was calculated since no synchronization with the neuronal event was carried out. In particular, $\mathbf{M}_H$ was obtained, as in Eq. (2), with the kernel iHRF equal to the SPM2 canonical hemodynamic response function. Activation maps are displayed for a statistical threshold, $P=.05$, corrected for family-wise error and with a minimum number of voxels in a cluster equal to 2. Activated areas were normalized to a standard brain by SPM2.

Both phase and magnitude SE EPI images were temporally high-pass filtered ($v_C=1/128$ Hz). No spatial smoothing was applied because in phase images, adjacent positive and negative variations could sum to zero for a symmetric configuration of the voxels with respect to the neuronal source and negative interference would occur in case of smoothing. The design matrix used in the linear regression comprised, in this case, both a modeled hemodynamic response, $\mathbf{M}_H$, and a neuronal response, $\mathbf{M}_N$ (see Eq. (1)), and effect sizes h and n were estimated. The kernel iHRF of Eqs. (2) and (3) was assumed to be equal to the SPM2 canonical hemodynamic response function for both magnitude and phase images; besides, $\mathbf{M}_N$, consisting of ones when the event occurred and zeros elsewhere (FIR model of order 1 and a window length equal to the TR; see Fig. 1). Activation maps are displayed for a statistical threshold, $P=.001$, uncorrected for multiple comparisons.

The temporal signal-to-noise ratio (SNR) was computed voxelwise on magnitude SE images after linear detrending (mean signal divided by its SD over time).

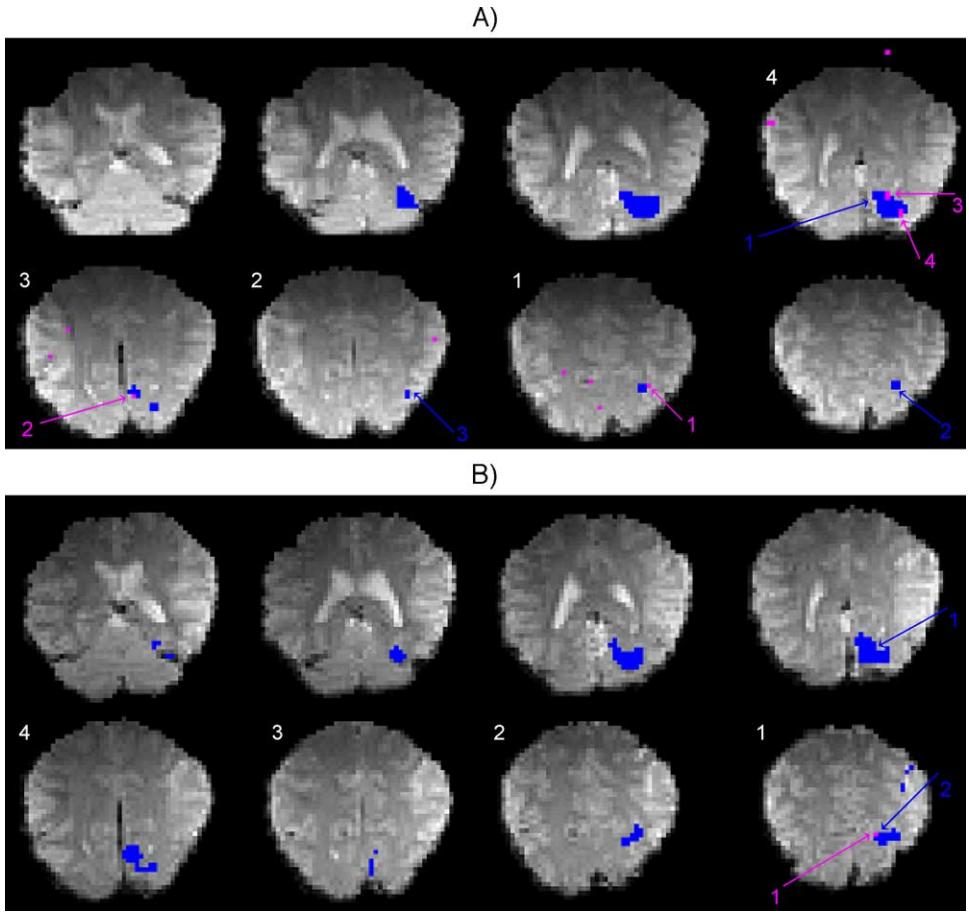

Fig. 5. BOLD activation patterns in GE and SE images for the subject investigated when using Design 2 (calibration of hemodynamic changes). In (A) and (B), for the first and second experimental sessions, respectively, superimposed on a BOLD GE magnitude image are shown: in blue and magenta, positively activated voxels corresponding to significant hemodynamic BOLD changes in GE and SE magnitude images, respectively ($P<.05$, corrected for family-wise error for GE results; $P<.001$, uncorrected for multiple comparisons for SE statistics). White numbers indicate the order of SE slice acquisition.

11. Results

11.1. VEP

The dipole modeling of the C1 component showed that the source activity is localized in the primary visual area V1 [Brodman area (BA) 17], at Talairach coordinates [9 −87 −4]. Its estimated dipole orientation, equal to [−0.11 −0.54 0.83] in Cartesian coordinates, is shown in Fig. 3A,B; the onset, peak and offset latencies of the source waveform (Fig. 2A) with respect to stimulus onset were 50, 76 and 115 ms, respectively.

11.2. BOLD contrast in GE magnitude images

BOLD GE activation patterns were detected in magnitude images of the investigated subject at both experimental measurements. Activation maps (blue-colored regions in Fig. 5A for the first session and in Fig. 5B for the second) were similar for both sessions and comprised areas pertaining both to striate (BA 17) and extrastriate (BA 18, BA 19) visual cortices. The cluster with the maximal statistical t value (indicated by N. 1 and a blue arrow in Fig. 5) comprised BA 17 (calcarine cortex) and BA 18 (around fusiform and lingual gyri), as verified after normalization to standard Talairach brain space; its t values were equal to 10.39 and 10.58 for the first and second experimental sessions, respectively ($Z_{equiv}=\infty$ for both), with corresponding numbers (n) of surviving voxels equal to 102 and 110. Activations were also found in the lateral occipital lobe (BA 19): around the superior occipital gyrus (cluster indicated by N. 2 and a blue arrow in Fig. 5A) with a t value equal to 6.47 ($Z_{equiv}=5.85$; $n=8$) and around the middle occipital gyrus (blue cluster N. 3 in Fig. 5A) with a t value equal to 4.88 ($Z_{equiv}=4.58$; $n=2$) for the first experimental session; only a single cluster located in the lateral occipital lobe with a t equal to 9.36 ($Z=7.78$; $n=43$; Fig. 5B) was identified at the second experimental session.

11.3. BOLD and neuronal current contrast in SE magnitude and phase images

Maximal temporal SNR values in the magnitude images were 54 and 37 for the first and second sessions, respectively.

BOLD contrast measured with Design 2, block design, yielded significant task-related hemodynamic changes in SE magnitude images located in visual areas in the form of multiple clusters comprising a single voxel (magenta-colored regions in Fig. 5A for the first session and in Fig. 5B for the second). In the first experimental session, four such activation clusters reached significance: the first two ($t=3.83$ and 3.66; with corresponding $Z_{equiv}=3.79$ and 3.62; Fig. 5a) were located in the lateral occipital lobe (around the superior and middle occipital gyri, respectively), and the next two clusters in BA 17–18 ($t=3.31$ and 3.24; with corresponding $Z_{equiv}=3.28$ and 3.21). For the second experimental session, only one voxel survived the statistical threshold, positioned in the lateral occipital lobe ($t=3.13$; $Z_{equiv}=3.10$, Fig. 5B). On the contrary, no significant hemodynamic BOLD signal changes were found in SE-phase images.

As shown in theory, the statistical efficiency to detect unwanted BOLD contrast present in Design 1 should be half of that measured with Design 2. Consequently, for the magnitude images of Design 1, maximal t values around

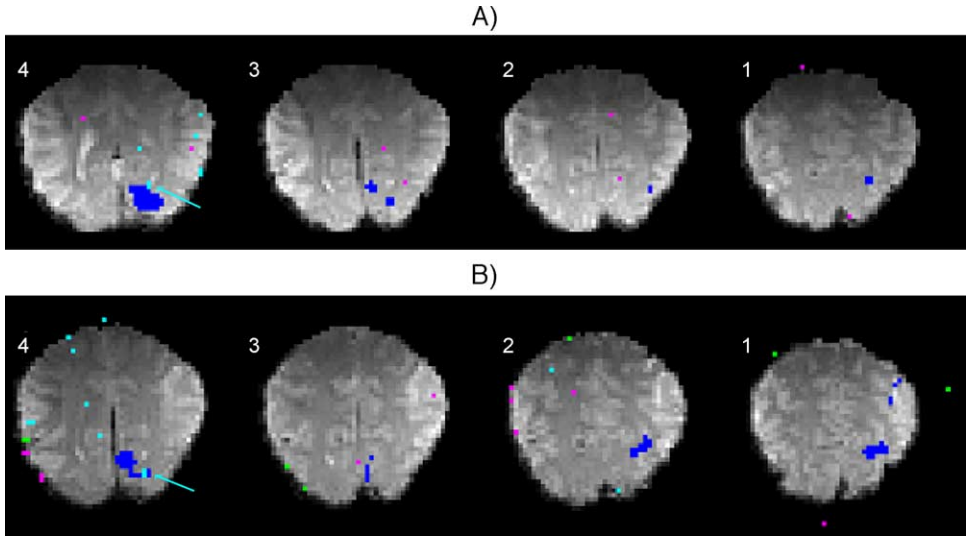

Fig. 6. Neuronal and hemodynamic activation patterns for the subject investigated when using Design 1 (detection of neuronal current effects). In (A) and (B), for the first and second experimental sessions, respectively, superimposed on a BOLD GE magnitude image are shown: in blue, positively activated voxels for BOLD GE magnitude images; in red/cyan, positively/negatively activated voxels in SE-phase images corresponding to neuronal event detection (fixed effects between two runs with ascending acquisition slice order); and in magenta/green, hemodynamic BOLD responses. White numbers indicate the order of SE slice acquisition. One neuronal-current activated voxel (indicated by the cyan arrow) resulted in visual area BA 17, near BOLD GE (and also SE) activations, although not exactly in the same location at each measurement session ($t=3.35$ and 3.58, phase variations equal to −11 and 4 mrad for the first and second experimental sessions, respectively). It pertains to a slice (4) obtained in synchrony with the presentation of the stimulus (together with Slice 2) (see Fig. 2C). In slices without prior stimulus presentation (Slices 3 and 4), no such significant signal variations could be observed.

1.6–1.9 were expected in BA 17–18 (with even lower t values in BA 19). This value is lower than the t threshold needed to achieve significance ($t=3.11$; significance level $P<.001$, uncorrected for multiple comparisons) and, therefore, no significant hemodynamic changes were expected in the magnitude or SE-phase images of Design 1. In line with theoretical predictions, no signal changes related to the BOLD contrast could be observed for this design ($t=3.11$) in visual areas, nor were there any for the first and second experimental sessions (see Fig. 6).

On the contrary, phase changes (decreases) related to the modeled neuronal currents were detected in visual areas (Fig. 6, green arrow), close to the brain regions showing BOLD activations in GE images (Cluster 1). Additional evidence, a necessary but not a sufficient condition, that the observed phenomenon is really due to neuronal currents and is not of non-neuronal origin is the slice [4] in which it occurred; indeed, this slice corresponds to the one where the MRI acquisition was synchronized with the presentation of the stimulus (together with Slice 2; for an ascending slice acquisition order, see Fig. 2C). However, concurrent activations (artefactual) in areas other than visual areas were present in the same slices and no neuronal current-induced phase changes in the opposite direction (increases) were found in voxels adjacent to these significant phase decreases.

With regard to magnitude images, no negatively activated voxels were found in visual areas for any of the runs (ascending and descending slice acquisition order), neither were there any in phase images (nor in the positive direction) for the second run (descending slice acquisition order).

12. Discussion

In the present study, a first attempt to detect in vivo primary magnetic effects of neuronal activity by SE MR images was conducted. A fundamental prerequisite for a successful application of neuronal current MRI is the discrimination between primary neuronal effects and secondary hemodynamic–metabolic changes. For this purpose, we chose to use SE instead of GE techniques because of their potential ability in this respect. However, in order to achieve in vivo detection of such primary magnetic field variations with SE techniques, the experimental approach had to be optimized with respect to the contrast-to-noise ratio and the recognizability of the phenomenon. With this aim, we propose an approach that combines different measurement modalities: EEG-based VEP recordings and conventional BOLD fMRI with SE MRI of neuronal current-induced magnetic field changes. In addition, by investigating the SE MRI time course in different experimental designs, we could further improve the precision of our approach.

The information related to the geometry (localization and orientation) of the dipolar source and its time evolution could be determined by VEP recordings. Knowledge of the dipolar source orientation was used to optimize the effect of the expected magnetic field variations on SE MR images by patient and slice positioning orthogonal to the dipolar source. With regard to orthogonalization of the dipole orientation to the external field, this condition could not always be achieved experimentally due to geometric constraints imposed by positioning inside the narrow bore of the MR scanner. In this context, it was possible to achieve some optimization by selection of a visual stimulus that facilitated subject positioning with regard to the geometry of the dipolar source. In a general perspective, such adaptations may limit the number of possible stimulation types that can be used in the experimental situation. While it is well known that the accuracy of the estimated dipole orientation and that of the temporal resolution of VEP recordings are exquisite, the spatial resolution may be of a more limited kind. Indeed, the localization of the dipolar source, by which neuronal current MRI slice positioning was guided, has an uncertainty of about 1 cm. For this reason, additional measurements of BOLD activation patterns were used in order to improve spatial localization of active regions in terms of the accompanying hemodynamic response. In this context, if possible, the acquisition of BOLD GE fMR images could be done in a distinct MRI experimental session, prior to the neuronal current SE measurement; this information could then be used as constraints for the spatial localization of the dipole estimated by the BESA algorithm. Hereby, the definition of the active regions, needed for SE MRI slice positioning and evaluation of neuronal current MRI activation patterns, would be improved.

Regarding the VEP component latencies obtained for a given subject and a specific stimulus, the TE of the SE sequence could be adapted to match the VEP time evolution. In this respect, a precise synchronization of the neuronal event with the MR SE acquisition had to be achieved by carefully triggering the stimulus at defined time points with respect to the MR sequence. Since the time course of the dipolar source is in the order of 100 ms, the time evolution of the first C1 peak could be accommodated between the excitation and the refocusing pulse of the SE sequence. Refocusing of the expected magnetic field changes was thus avoided and, thereby, the achievable CNR was increased. Besides, longer TEs also affect the SNR; however, at 1.5 T, the selected TE is in the order of the transverse relaxation time in gray matter and a satisfying trade-off between CNR and SNR could be obtained. The precise synchronization, within limits given by physiological variation of the VEP signal time course and stimulus delivery, was also used to verify that neuronal currents really caused the observed signal changes by an additional method: for each experimental run, the stimulus was presented prior to acquisition of every second slice only, which were shifted between runs to cover the active brain region. Indeed, significant signal changes were

observed in the stimulated slices alone, thereby adding some confidence to our observations.

Beyond spatiotemporal synchronization of stimulus presentation with MR acquisition, there is another relevant issue: it regards the control of artefactual contributions of non-neuronal origin to the signal, especially in terms of stimulus-induced hemodynamic changes, which constitute the BOLD signal itself. In the present paper, neuronal and hemodynamic responses were modeled as two distinct contributions that add linearly to the signal (although the neuronal signal also modulates the hemodynamic effect); in this context, a stimulus timing (Design 1) was suggested and applied experimentally in vivo, which allowed concurrent estimation of both neuronal and hemodynamic effects, rendering them decorrelated and, hence, estimable. The adoption of a high-frequency design (1 scan ON/2 scans OFF cycle) gave a suitable solution to the problem, although a complete decorrelation was not achieved. In a previous study, Xiong et al. [6] also adopted a high-frequency design (1 scan ON/1 scan OFF), although the stimulus-correlated signal was acquired at the Nyquist frequency, which inevitably will lead to some loss of detection power. Other solutions for decorrelating the neuronal and nonneuronal contributions can be found in the time domain. For example, by the use of designs for which the distribution of the $\mathbf{M}_N \otimes$ I-HRF term is normal, like latin-square designs or geometric designs, as suggested for conventional BOLD fMRI studies [17]. In addition, the use of *m* sequences has been proposed [18] to disentangle fast (neuronal and other effects) from slow (e.g., BOLD) responses, neglecting the other component, $\mathbf{M}_N$, which we believe to contribute independently to the signal. *M* sequences were originally introduced in fMRI studies to efficiently estimate the shape of the hemodynamic responses in fast event-related experiments [19]; however, they suffer from low detection efficiency for both first- and second-order responses, as noted by Kellman et al. [20], in order to disentangle fast neuronal nonlinearities from hemodynamic effects.

Some results from the pilot study shown in the present work are encouraging. They indicate that magnetic effects caused by neuronal currents may be detected in vivo by SE-phase MRI; indeed, these changes were carefully synchronized with the acquisition and could be registered close to brain regions recorded as active by VEP and conventional BOLD fMRI. Since these changes were observed in phase and not magnitude images, our data seem to support the model of an extended oriented dipole, with measurable effects within the dimension of the MRI voxel, as predicted by Konn et al. [3]. This dipole corresponds to the source of scalp potential recordings obtained by EEG (MEG), which is generally related to the extra(intra-)cellular current of apical dendrites pertaining to pyramidal cells, oriented radially (tangentially) to the scalp. The estimated dipole intensity of 50 nAm in the primary visual cortex of the subject investigated, in relation to previous calculations regarding extended dipoles [3], actually may induce MR-detectable phase changes.

In the future, more work has to be done to further validate detection of primary magnetic effects caused by neuronal currents. In particular, results should be reproduced for more subjects and different stimulation types; besides, more precise modeling of the neuronal processes should be performed in order to account for the different dipolar geometries of dendrites pertaining to both pyramidal and non-pyramidal cells.

Acknowledgments

This work was supported by the Italian Ministry of Health (RC04F).

References

[1] Bodurka J, Jesmanowicz A, Hyde JS, Xu H, Estkowski L, Li SJ. Current-induced magnetic resonance phase imaging. J Magn Reson 1999;137:265–71.

[2] Bodurka J, Bandettini PA. Toward direct mapping of neuronal activity: MRI detection of ultraweak, transient magnetic field changes. Magn Reson Med 2002;47:1052–8.

[3] Konn D, Gowland P, Bowtell R. MRI detection of weak magnetic fields due to an extended current dipole in a conducting sphere: a model for direct detection of neuronal currents in the brain. Magn Reson Med 2003;50:40–9.

[4] Bianciardi M, Cerasa A, Maraviglia B, Hagberg GE. On the detection limit of current induced phase changes in magnetic resonance imaging at 1.5 T: single- versus multi-spin-echo techniques. Neuroimage 2004;22(Suppl. 1):S57 [poster N. 258].

[5] Petridou N, Plenz D, Bodurka J, Bandettini PA. Neuronal current MR imaging in vitro. Neuroimage 2003;19(Suppl. 2):S40.

[6] Xiong J, Fox PT, Gao JH. Directly mapping magnetic field effects of neuronal activity by magnetic resonance imaging. Hum Brain Mapp 2003;20:41–9.

[7] Kamei H, Iramina K, Yoshikawa K, Ueno S. Neuronal current distribution imaging using magnetic resonance. IEEE Trans Magn 1999;35:4109–11.

[8] Yacoub E, Duong TQ, Van De Moortele PF, Lindquist M, Adriany G, Kim SG, et al. Spin-echo fMRI in humans using high spatial resolutions and high magnetic fields. Magn Reson Med 2003; 49:655–64.

[9] Oja JME, Gillen J, Kauppinen RA, Kraut M, van Zijl PCM. Venous blood effects in spin-echo fMRI of human brain. Magn Reson Med 1999;42:617–26.

[10] Friston KJ, Holmes AP, Poline JB, Grasby PJ, Williams SCR, Frackowiak RSJ, et al. Analysis of fMRI time-series revisited. Neuroimage 1995;2:45–53.

[11] Boynton GM, Engel SA, Glover GH, Heeger DJ. Linear systems analysis of functional magnetic resonance imaging in human V1. J Neurosci 1996;16:4207–21.

[12] Aguirre GK, Zarahn E, D'Esposito M. The variability of human, BOLD hemodynamic responses. Neuroimage 1998;8:360–9.

[13] Elliott MA, Bloy L, Gualtieri EE, Hulvershorn J, Leigh JS. Estimation of the temporal resolving power of spin echo and gradient echo fMRI at 3 T. Neuroimage 2004;22(Suppl. 1):S57 [poster N. 274].

[14] Hulvershorn J, Bloy L, Gualtieri EE, Leigh JS, Elliott MA. Using peak hemodynamic activation time as a measure of spatial sensitivity in spin echo fMRI. Neuroimage 2004;22(Suppl. 1):S57 [poster N. 291].

[15] Kiselev VG, Posse S. Analytical model of susceptibility-induced MR signal dephasing: effect of diffusion in a microvascular network. Magn Reson Med 1999;41:499–509.
[16] Di Russo F, Martinez A, Sereno MI, Pitzalis S, Hillyard SA. Cortical sources of the early components of the visual evoked potential. Hum Brain Mapp 2001;15:95–111.
[17] Bianciardi M, Cerasa A, Patria F, Hagberg GE. Evaluation of mixed effects in event-related fMRI studies: impact of first-level design and filtering. Neuroimage 2004;22:1351–70.
[18] Fukunaga M, de Zwart JA, van Gelderen P, Chu R, Kellman P, Duyn JH. Hunting for neuronal currents: absence of rapid MRI signal changes during visual evoked response. Neuroimage 2004;22 (Suppl. 1):S57 [poster N. 279].
[19] Buracas GT, Boynton GM. Efficient design of event-related fMRI experiments using M-sequences. Neuroimage 2002;16:801–13.
[20] Kellman P, Gelderen P, de Zwart JA, Duyn JH. Method for functional MRI mapping of nonlinear response. Neuroimage 2003; 19:190–9.